Thermodynamic Analysis of an Integrated Gasification Solid Oxide Fuel Cell Plant with a Kalina Cycle

Pierobon, Leonardo; Rokni, Marvin Mikael

Published in:
International Journal of Green Energy

Link to article, DOI:
10.1080/15435075.2013.867267

Publication date:
2015

Document Version
Peer reviewed version

Pierobon, L. and **Rokni, M.** Thermodynamic Analysis of an Integrated Gasification Solid Oxide Fuel Cell Plant with a Kalina Cycle. *Int J Green Energy* 2015:12;610 -619.

Thermodynamic Analysis of an Integrated Gasification Solid Oxide Fuel Cell Plant with a Kalina Cycle

Leonardo Pierobon and Masoud Rokni
Technical University of Denmark, Department of Mechanical Engineering,
Building 403, DK-2800 Kgs. Lyngby, Denmark

Abstract

A hybrid plant that consists of a gasification system, Solid Oxide Fuel Cells (SOFC) and a Simple Kalina Cycle (SKC) is investigated. Woodchips are introduced into a fixed bed gasification plant to produce syngas, which is then fed into an integrated SOFC-SKC plant to produce electricity. The pre-treated fuel then enters the anode side of the SOFC. Complete fuel oxidation is ensured in a burner by off-gases exiting the SOFC stacks. Off-gases are utilized as heat source for a SKC where a mixture of ammonia and water is expanded in a turbine to produce additional electric power. Thus, a triple novel system based on a gasification plant, a SOFC plant and a SKC plant is presented and investigated. The system is called IGSKC (Integrated Gasification SOFC Simple Kalina Cycle). The system layout is studied, and the optimal ammonia-water mole fraction is selected. An electrical efficiency of 58% is achieved; plant size and nominal power are selected based on the required cultivation area.

SOFC heat recovery with SKC is compared to a Steam Cycle (SC). Although ammonia-water more accurately fits the temperature profile of the off-gases, the presence of a Hybrid Recuperator enhances the available work in the SC case, resulting in a higher overall thermal efficiency.

Keywords: SOFC, Kalina, gasification, hybrid recuperator, water-ammonia, alternative plant

1. Introduction

Biomass utilization for electric generation is poor in terms of thermal efficiency. Rankine cycle plants with electric power outputs of approximately 10-20 MW have efficiencies of approximately 25-28%. For smaller demands, (5-1000 kW) ORC (Organic Rankine Cycle) and Stirling engines can be used and performance may also be decreased (Cocco et al. 2010). Technologies based on wood gasification will soon reach the market which then will allow the conversion of lignocellulosic biomass into a gaseous medium that can be used for electric power generation combined with a fuel cell plant. SOFC is an electrochemical reactor currently under development by some companies for power and heat generation applications. In recent years, development of solid oxide fuel cells operated in the intermediate temperature range of 600–800°C has received much attention as potential for high-efficiency power generation systems see e.g. Rose et al. (2009) and Kim et al. (2009). For example Liso et al. (2009) among many presented a small scale cogeneration (heat and power) system based on intermediate temperature SOFC with high efficiency.

In the literature, many combinations of SOFC and conventional power plants have been demonstrated, e.g., Pålsson et al. (2000) for producing combined heat and power (CHP) and

Proell et al. (2004) with internal biomass gasification. Characterization, quantification and optimization of hybrid SOFC-GT (Gas Turbine) systems have been studied by, e.g., Subramanyan and Diwekar (2005) and Calise et al. (2006). Bang-Møller et al. (2011) studied a hybrid plant that produced CHP (Combined Heat and Power) from biomass using a two-stage gasification concept, a solid oxide fuel cell (SOFC) plant and a micro gas turbine. In hybrid SOFC-GT plants, the SOFC stacks must be pressurized in an extremely large vessel (depending on the size of the plant, which is usually a megawatt-class facility). Such a practical problem will be diminished in hybrid SOFC-SC systems because the stacks will function under atmospheric pressure. Another disadvantage of a SOFC-GT system is that the startup simplicity of the GT is diminished because the startup time of a SOFC plant is much longer than a GT plant. In addition, SOFC manufacturers are trying to decrease the operating temperature of the SOFC stacks; then, a SOFC-SC hybrid system would be more attractive than the SOFC-GT systems.

Investigations of combined SOFC and steam cycle plants were first carried out by Dunbar et al. (1991). Later, Rokni (2010) presented an integrated system consisting of SOFC and a steam cycle fired by natural gas with a thermal efficiency of up to 62%. A triple hybrid plant (IGSS) fueled by woodchips and based on a gasification plant, a SOFC plant and a SC is analyzed and optimized for electric power production in Rokni and Pierobon (2011) and Rokni (2012). The performance of an integrated gasification plant with SOFC, GT and SC was also studied in e.g. Odukoya et al. (2011). A reasonable size of a pure biomass plant is approximately 5-50 MW, requiring a cultivation area of 20-125 km^2 (see Cocco et al., 2010); this restricts the steam turbine size, causing a low duct flow area and, therefore, a lower isentropic efficiency. In IGSS, an appropriate live steam pressure must be selected to avoid high moisture contents at the turbine outlet, which would cause blade corrosion over the long term.

In a study by Ghirardo et al. (2011), the heat-recovery is derived from an ORC running on diathermic oil; this solution is considered viable for use on ships. The thermal efficiency is approximately 49%; such a low value is related to the exergy loss experienced during the heat exchange between the SOFC plant off-gases and the ORC working fluid. Exergy losses occur due to vaporization occurring at constant temperature and to the relatively low maximum cycle temperature (approximately 279°C, Ghirardo et al., 2011). In this sense, the use of a Kalina Cycle (KC) as the heat recovery unit is potentially able to decrease the exergy losses because the working fluid, i.e., the ammonia-water mixture, involves vaporization with a variable temperature profile. In the literature, many studies that address the thermodynamic performance of KC are available; in Marston (1990), gas turbine waste heat is recovered in a KC with a cycle efficiency of 32-33% and with an off-gas maximum temperature of 550°C. Jonnson and Yan (2000) showed results from a recuperating diesel engine heat power, and Di Pippo, (2004) showed a detailed comparison between KC and ORC in geothermal applications. It should be noted the following Kalina cycles were built and operated; Canoga Park (in California, USA), Fukuoka (in Kyushu, Japan), Sumitomo Steel (Tokyo, Japan) and Husavik (in Iceland). Recently, Zhang et al. (2012) presented a review research on the Kalina cycles and reported that copper based alloys suffer of corrosion in presence of ammonia causing oxidation of bearing and other components. They also reported that mild steel and aluminium seem to be inappropriate materials for Kalina cycle systems but several stainless steels (304, 316, nitronic 60 and duplex) as well as 6Al–4V titanium do not appear to suffer from corrosion.

This study is aimed at presenting a new system to be fueled by woodchips composed of a gasification plant, a SOFC system and a SKC plant; therefore, the current investigation is novel in terms of alternative power plants for future applications. The ammonia-water mixture model is based on the most recent correlation found by Tillner-Roth and Friend (1998) from

experimental data for temperature and pressure up to 810 K and 40 MPa, respectively. An optimized system is selected based on the SOFC operative temperature, the ammonia-water mole fraction and the SKC maximum pressure. A comparison between the optimized IGSKC and IGSS is presented and discussed for a future scenario.

2. Methodology

The results of this paper are found using the simulation tool DNA (see e.g. Elmegaard and Houbak, 2005), which is a simulation tool for energy systems analyses. In DNA, the physical model is formulated by connecting the relevant component models through nodes and by including operating conditions for the complete system. The physical model is converted into a set of mathematical equations to be solved numerically. The mathematical equations include mass and energy conservation for all components and nodes, as well as relationships for the thermodynamic properties of the fluids involved. The component library includes models of heat exchangers, burners, gasifiers, turbo machinery, dryers and decanters, energy storages, engines, valves and controllers, as well as more specialized components and utility components. The user may also implement additional components.

2.1 Thermodynamic modeling of ammonia-water mixture

Ammonia-water mixture was added as a new fluid in the DNA library to simulate the entire system with different boundary conditions. In recent years, several models have been developed to calculate the properties of ammonia-water mixtures. In Klein and Ibrahim (1993), correlations are implemented for temperatures and pressures up to 600 K and 11 MPa, respectively. Park and Sonntag (1990) applied a Benedict-Webb-Rubin (BWR) equation of state for pressures up to 20 MPa and a temperature of approximately 650 K. In this paper, the Tillner-Roth and Friend (1998) formulation based on Helmholtz free energy is implemented and compared with experimental data found in the literature. This approach allows thermodynamic calculations for all ammonia-water properties with uncertainties of ±0.1-0.3% for density and ±200 J mol^{-1} for enthalpies in the single phase regions. The fundamental equation of state for Helmholtz free energy (A = U – TS) for a binary mixture is expressed by

$$\frac{\overline{A}}{R_m} = \phi = \phi^0\left(\tau^0, \delta^0, x\right) + \phi^r\left(\tau, \delta, x\right) \tag{1}$$

where ϕ^0 is the ideal term that depends on dimensionless temperature τ^0, specific volume δ^0 and ammonia mole fraction x, and the residual term ϕ_r depends on $\tau = T/T_n$ and $\delta = V/V_n$. The ideal part ϕ^0 is given as a linear combination of water and ammonia ideal gases ϕ_{10} and ϕ_{20}, adding the two terms that result from the entropy of mixing in the ideal mixture. For a given T, V and composition, the equation is

$$\phi(T,V,x) = (1-x)\phi_{01}^0\left(\tau_{01}^0, \delta_{01}^0\right) + x\phi_{02}^0\left(\tau_{02}^0, \delta_{02}^0\right) + (1-x)\ln(1-x) + x\ln x \tag{2}$$

The residual term ϕ_r has the form

$$\phi^r\left(\tau, \delta, x\right) = (1-x)\phi_{01}^r\left(\tau, \delta\right) + x\phi_{02}^r\left(\tau, \delta\right) + \Delta\phi^r\left(\tau, \delta, x\right) \tag{3}$$

where ϕ_{r01} and ϕ_{r02} are the residual contributions of water and ammonia, respectively, the full equations for which are acquired from Pruβ and Wagner (1995) and Tillner-Roth et al. (1993). To adjust the calculations to the experimental data, an empirical departure function is added. Fig. 1(a) compares the bubble point pressures as a function of mixture composition between the results from DNA-implemented software and experimental data for temperatures from 300 to 400 K (Table 4 in Tillner-Roth and Friend 1998); the highest relative error is approximately 2%. Fig. 1(b) shows the enthalpy-temperature schedule at a constant pressure (1 bar) in the superheated vapor region for different ammonia-water concentrations. It can be noted that the relative errors are on the order of 0.4%. The behavior of the equation of state can be extended up to 810 K; however, the accuracy is not predicted because no data were available in that region.

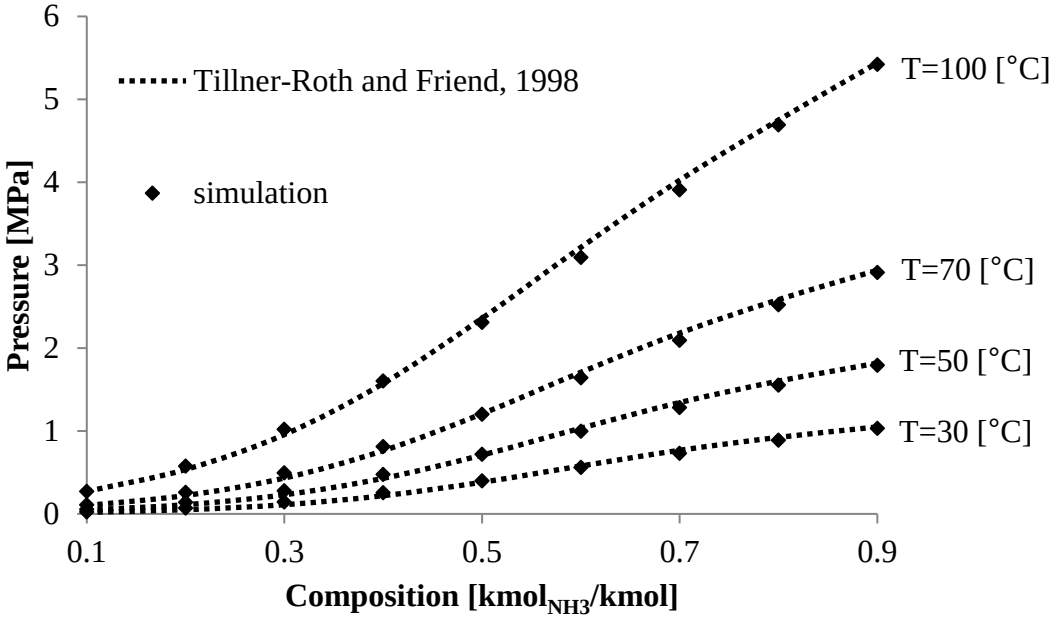

(a)

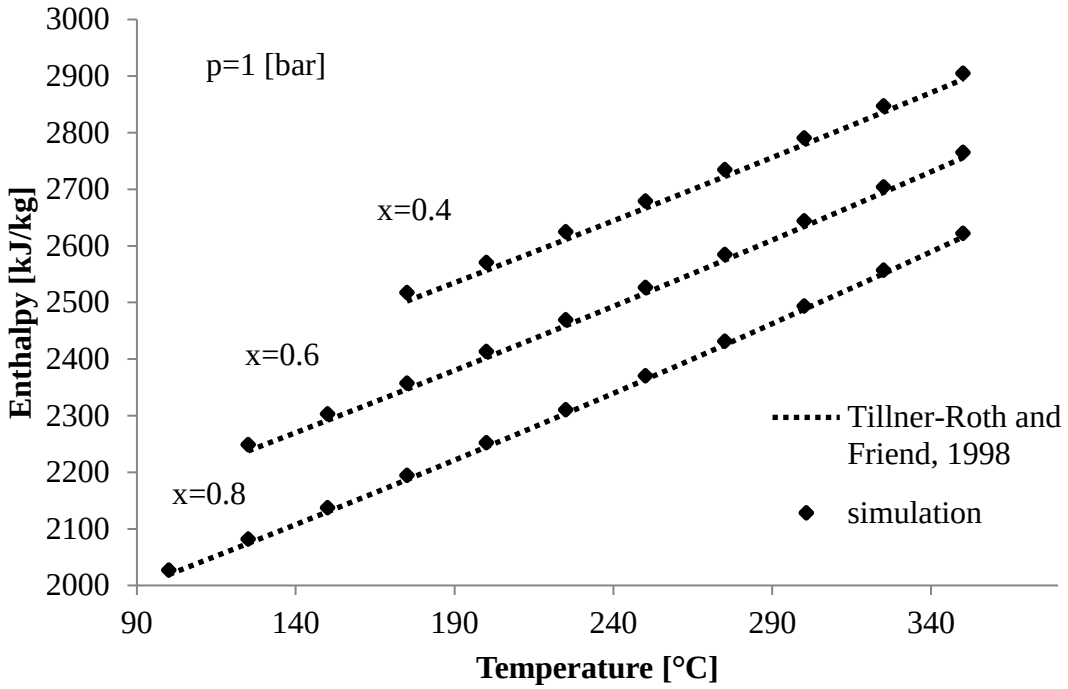

(b)

Figure 1. (a) Vapor enthalpy vs. temperature for different mixture compositions (constant pressure); (b) Saturated liquid pressure vs. composition for different mixture temperatures

Finally, it should be noted that DNA calls for thermodynamic properties with different combinations of variables, e.g., f(P,T,x), f(H,P,x), f(P, quality, x). Because the Helmholtz free energy is in an explicit form only when temperature, volume and mixture composition are specified, an iteration scheme is thus implemented using DNA. The procedure is carried out using a Regula Falsi algorithm for each set of variables based on the following iteration scheme:

$$X_{n+1} = X_n - F(X_n, Y_n)\frac{(X_n - X_{n-1})}{F(X_n, Y_n) - F(X_{n-1}, Y_{n-1})} \tag{4}$$

2.2 Gasifier modeling

A two-stage Viking gasifier was used in this investigation. This 75 kW_{th} gasifier was demonstrated at the Risø-Technical University of Denmark (Henriksen et al., 2006). The processes of pyrolysis and gasification were divided into two separate reactors, as shown in Fig. 2. Wet biomass (woodchips) was fed into the first reactor where drying and pyrolysis took place before the pyrolysis products (600°C) were fed to a downdraft fixed bed char gasifier, which was the second reactor. The exhaust gases from the gasifier were then used to heat the reactor for drying and pyrolysis, as seen in the steam loop in Fig. 2. Between pyrolysis and char gasification, partial oxidation of the pyrolysis products provided heat for the endothermic char gasification reactions. Char was gasified in the fixed bed while H_2O and CO_2 acted as gasifying agents in the char gasification reactions. The Viking gasifier operated near atmospheric pressure.

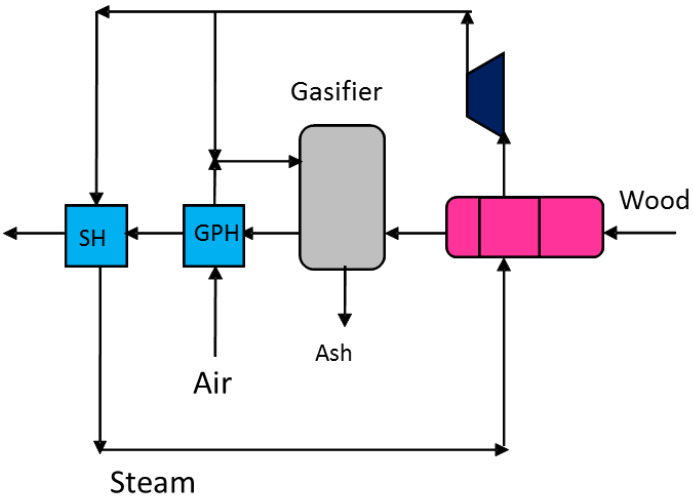

Figure 2. Layout of the two-stage gasification plant
GPH=gasifier preheater, SH=steam heater

A simple Gibbs reactor model is used to model the gasifier (see Smith et al., 2005), which means that the total Gibbs free energy is at its minimum when chemical equilibrium is achieved. This characteristic is used to calculate the gas composition at a specified temperature and pressure without considering the reaction paths. The procedure is briefly described here. The Gibbs free energy of a gas (assumed to be a mixture of *k* perfect gases) is given as

$$\dot{G} = \sum_{i=1}^{k} \dot{n}_i \left[g_i^0 + RT \ln(n_i p) \right] \tag{5}$$

where g^0, R and T are the specific Gibbs free energy, universal gas constant and gas temperature, respectively. Each atomic element in the inlet gas is in balance with the outlet gas composition, which means that the flow of each atom has to be conserved. For *N* elements, this is expressed as (see e.g. Elmegaard and Houbak, 1999)

$$\sum_{i=1}^{k} \dot{n}_{i,in} \mathbf{A}_{ij} = \sum_{m=1}^{w} \dot{n}_{m,out} \mathbf{A}_{mj} \qquad \text{for } j = 1,N \tag{6}$$

The *N* elements correspond to H_2, O_2, N_2, CO, NO, CO_2, steam, NH_3, H_2S, SO_2, CH_4, C, NO_2, HCN (hydrogen cyanide), COS (carbonyl sulfide), Ar and ash (SiO_2) in the gasifying process. $\mathbf{A}_{mj}$ is the number of atoms of element *j* (H, C, O, N) in each molecule of entering compound *i* (H_2, CH_4, CO, CO_2, H_2O, O_2, N_2 and Ar), while $\mathbf{A}_{ij}$ is the number of atoms of element *j* in each molecule of leaving compound *m* (H_2, O_2, N_2, CO, NO, CO_2, steam, NH_3, H_2S, SO_2, CH_4, C, NO_2, HCN (hydrogen cyanide), COS, Ar and ash). The minimization of the Gibbs free energy can be found by introducing a Lagrange multiplier, μ, for each of the N constraints obtained in Eq. (15). After adding the constraints, the expression to be minimized is then

$$\phi = \dot{G}_{tot,out} + \sum_{j=1}^{N} \mu_j \left(\sum_{i=1}^{k} \dot{n}_{i,out} A_{ij} - \sum_{m=1}^{w} \dot{n}_{m,in} A_{mj} \right) \tag{7}$$

The partial derivative of this equation with respect to $\dot{n}_{i,out}$ can be written as

$$\frac{\partial \phi}{\partial \dot{n}_{i,out}} = \frac{g^0_{i,out}}{RT} + \ln\left(n_{i,out} p_{out}\right) + \sum_{j=1}^{k} \mu_j \mathbf{A}_{ij} \qquad \text{for } i = 1, k \tag{8}$$

At the minimum, each of these is then zero.

2.3 SOFC modeling

The SOFC model used in this investigation is based on the model developed by Bang-Møller and Rokni (2010), which was calibrated against experimental data for the planar type SOFC. For the sake of clarity, it is shortly described here. The model is a zero-dimensional model which enables calculating complicated energy systems. In such modeling one must distinguish between electrochemical modeling, calculation of cell irreversibility (cell voltage efficiency) and the species compositions at outlet. For electrochemical modeling, the operational voltage (E_{cell}) was found to be

$$E_{cell} = E_{Nernst} - \Delta E_{act} - \Delta E_{ohm} - \Delta E_{conc} - \Delta E_{offset} \tag{9}$$

where E_{Nernst}, ΔE_{act}, ΔE_{ohm}, ΔE_{conc} and ΔE_{offset} are the Nernst ideal reversible voltage, activation polarization, ohmic polarization, concentration polarization and the offset polarization, respectively. In this study, the offset polarization is neglected because its contribution is very small. Assuming that only hydrogen is electrochemically converted, the Nernst equation will be given as

$$E_{Nernst} = \frac{-\Delta g_f{}^0}{n_e F} + \frac{RT}{n_e F} \ln\left(\frac{p_{H_2,tot} \sqrt{p_{O_2}}}{p_{H_2O}} \right), \tag{10}$$

$$p_{H2,tot} = p_{H2} + p_{CO} + 4 p_{CH4} \tag{11}$$

where Δg_f^0 is the Gibbs free energy (for the reaction of H_2) at standard pressure. The water-gas shift reaction is very fast, which therefore justifies the assumption of hydrogen as the only species to be electrochemically converted.

The activation overpotential is due to an energy barrier (activation energy) that the reacting species must overcome in order to drive the electrochemical reactions. The activation overpotential of each electrode is a non-linear function of the current density and is usually expressed by the Butler-Volmer equation equation see Keegan et al. (2002). The total activation overpotential in this model is hereby defined as the sum of the activation overpotential of each electrode, anode and cathode.

The ohmic overpotential is caused by the ohmic resistance towards the oxygen ions passing through the electrolyte and the electrons passing through the electrodes and interconnects. The ohmic overpotential is dominated by the resistance in the ion conducting electrolyte. The anodic and cathodic current densities are calculated from Zhu and Kee (2003) and Achenbach (1994), respectively.

The concentration overpotential is a result of the limitations of diffusive transport of reactants and products between the flow channel and the electrode-electrolyte interface. The effect is increasing with current density and at a certain current density limit this transport of species is not fast enough to feed the electrochemical reactions taking place and the partial

pressure of reactants at the electrode-electrolyte interface approaches zero. The anode and cathode current density limits are different and they are dependent on microstructural characteristics of the respective electrode and operating conditions of the SOFC, see e.g. Kim and Virkar (1999).

The fuel composition leaving the anode is calculated by the Gibbs minimization method as described in Smith et al. (2005). Equilibrium is assumed for the anode outlet temperature and pressure for the following species: H_2, CO, CO_2, H_2O, CH_4 and N_2. Thus, the Gibbs minimization method calculates the compositions of these species at the outlet by minimizing their Gibbs energies. The equilibrium assumption is reasonable because the methane content in this study is sufficiently low.

To calculate the voltage efficiency of the SOFC cells, the power production from the SOFC (P_{SOFC}) depends on the amount of chemical energy fed to the anode, the reversible efficiency (η_{rev}), the voltage efficiency (η_v) and the fuel utilization factor (U_F). The details can be found in Rokni (2012).

2.4 Simple Kalina Cycle (SKC)

In this study, a simple Kalina cycle is proposed to operate with a fixed ammonia-water mixture. The need for separator and problems associated with external heat supply is thus eliminated. If the Kalina plant was intended to operate with different ammonia solutions, then the system design would slightly be different from the one proposed here, see Leibowitz and Mirolli (1997) for details. In Fig. 3, a SKC runs on an ammonia-water mixture as its working fluid; it is composed of an ammonia-water steam generator divided into an evaporator (EVA) and a superheater (SUP). The mixture is then sent to a Kalina Turbine (KT), where mechanical power is produced and converted into electricity by an electrical generator. The KT outlet mixture cools down through the Kalina Regenerator (KRG), where the pumped medium is heated and partially vaporized before entering the EVA. A condenser and mixture pump complete the whole cycle.

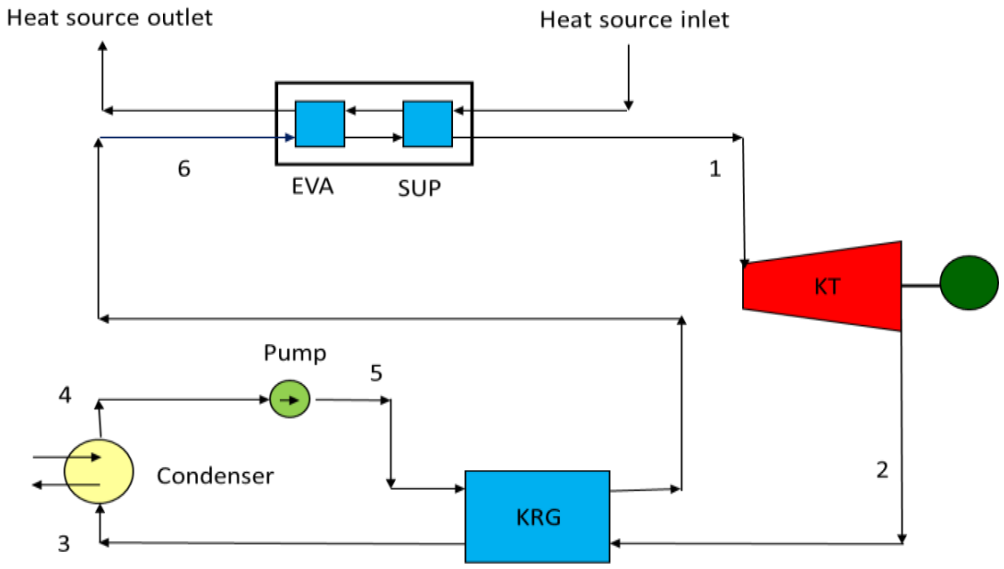

Figure 3. Layout of simple Kalina cycle
EVA=evaporator, KRG=Kalina regenerator, KT=Kalina turbine, SUP=super heater

Table 1. Input parameters for SKC (simple Kalina cycle) simulation

Parameter	
Power output	1 [MW]
Mixture composition	0.7 [mol(NH_3)/mol]
Turbine inlet temperature	250 [°C] (ref. Lai et al., 2011)
Turbine outlet pressure	23.4 [bar]
Turbine outlet pressure	6.3 [bar]
Condenser inlet temperature	58 [°C]
Isentropic efficiency	0.85 [-] (ref. Lai et al., 2011)
Electric generator efficiency	0.96 [-]
Pump efficiency	0.65 [-] (ref. Lai et al., 2011)
Heat exchanger pressure losses	0.01 [bar]

A SKC is simulated to compare its potential as a waste heat recovery unit with present and future technologies under investigation; in particular, the results reported by Lai et al. (2011) for subcritical and supercritical ORC are used for comparison. Simulations are carried out with the parameters listed in Table 1. According to Lai et al. (2011), a maximum temperature of 250°C is selected. It must be noted that the restriction on the minimum condenser temperature (38°C) is also respected because the inlet and outlet ammonia-water condenser temperatures (points 4 and 3) are 25°C and 58°C, respectively.

Figure 4 shows an example of the T–S diagram resulting from the SKC simulation. It can be noted that the mixture enters the EVA with a mixture quality of approximately 0.43 (point 6). The variable vaporization temperature decreases the exergy losses associated to the HRSG (Heat Recovery Steam Generator) and thereby increases the mean thermodynamic temperature which in turn results in a higher thermal efficiency when compared to the case that vaporization temperature is constant (e.g. pure water is the working fluid). The inlet turbine temperature (point 1) is 250°C. The KT outlet (point 2) ends up being far from the saturation curve; therefore, the turbine blades do not suffer damage and corrosion due to partial condensation. Heat is exchanged internally in the KRG when the pumped mixture is heated (from 5 to 6) by cooling down the exhaust vapor leaving the KT; this technique allows the enhancement of the EVA inlet temperature, resulting in a further performance increase.

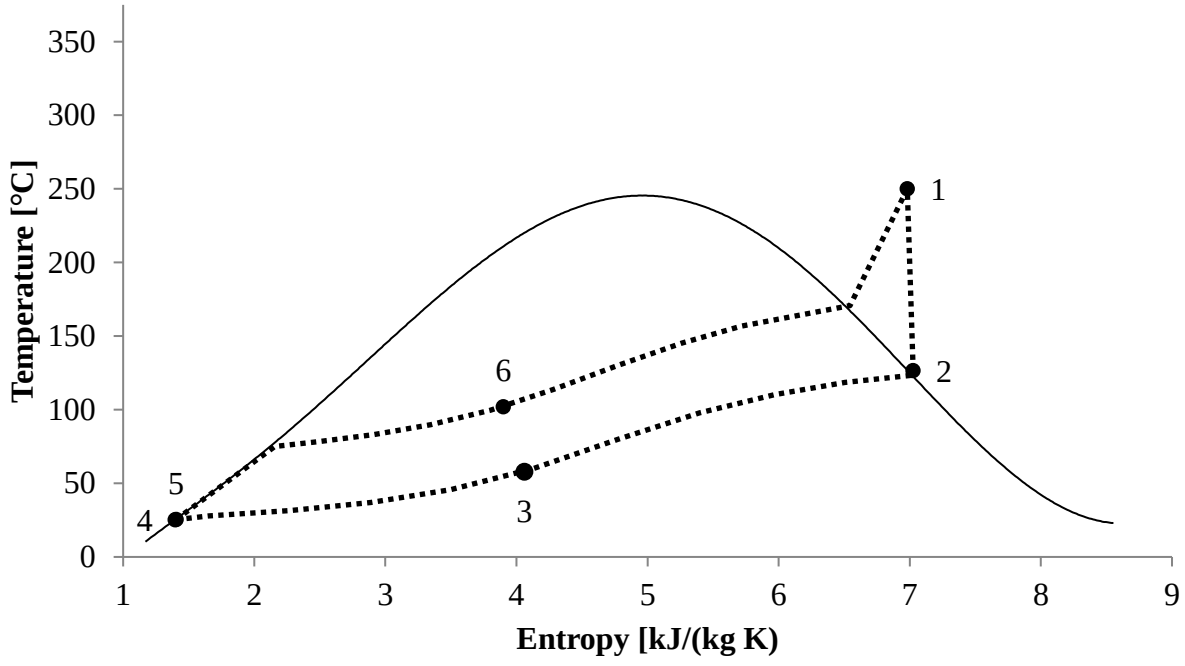

Figure 4. T–S (temperature – entropy) diagram of simulated simple Kalina cycle

Results from the DNA simulations are listed in Table 2. The thermal efficiency of the cycle is calculated by the following equation:

$$\eta_{thSKC} = 100 \frac{P_{KT} - P_{pump}}{\dot{q}_{in,SKC}} \tag{12}$$

where P_{KT}, P_{pump} and $\dot{q}_{in,SKC}$ are Kalina turbine power generated, Kalina cycle pump power consumption and incoming heat to the SKC plant from the off-gases of the SOFC cycle, respectively.

Table 2. Obtained results from the SKC (simple Kalina cycle) simulation

Results	
Mass flow	4.13 [kg/s]
Turbine outlet temperature	126.1 [°C]
Condenser inlet quality	0.49 [kg(v)/kg]
Condenser outlet temperature	25 [°C]
Heat power input	5.0 [MW]
Auxiliary power consumption	0.016 [MW]
Power output	1.0 [MW]
Thermal efficiency	20.03 [%]

Figure 5 shows the ammonia-water temperature profile inside the KRG and condenser vs. heat exchanged. The outlet turbine temperature (point 2) is approximately 126.1 °C. Condensation occurs at a variable temperature between 58°C and 25°C with a mixture quality decreasing from 0.49 to pure liquid.

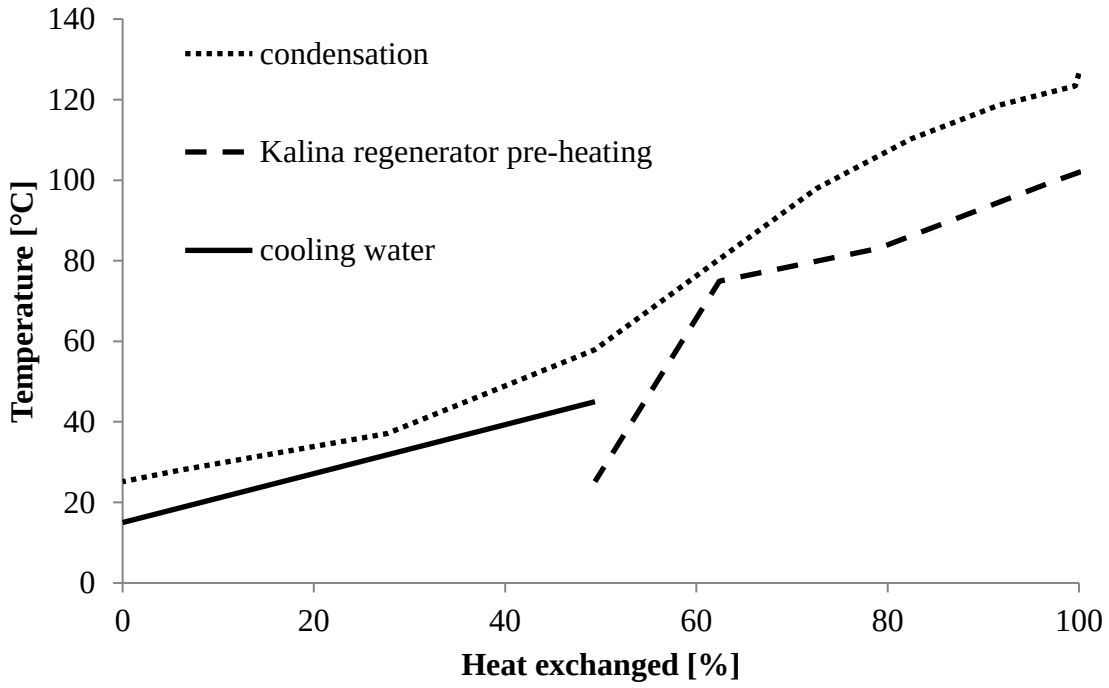

Figure 5. KRG (Kalina regenerator) and condenser temperature profile vs. heat exchanged

Figure 5 also indicates that increasing the maximum pressure of the working fluid could cause the KRG pre-heating line to move upwards and eventually cross the line of the condensation, which is then physically not correct. In the analysis, a pinch point of 10°C is kept as the limit when analysing these lines. Table 3 shows the ORC thermal efficiencies for n-Pentane in both subcritical and supercritical configurations with a regenerator included in the system layout. It can be noted that SKC is a valid alternative for low and medium temperature heat recovery because it presents a higher thermal efficiency (20.0%) when compared to both subcritical and supercritical n-Pentane ORC. An advantage of SKC is that the heat acquired from the power source is partially exchanged with a two phase mixture (EVA) and with superheated fluid (SUP), whereas the supercritical ORC deals entirely with a working medium in the superheated region, which requires a wider heat exchange area for a given temperature profile. The maximum pressure is also lowered, which decreases material stress.

Table 3. Comparison between subcritical and supercritical n-Pentane ORC (organic Rankine cycle), form ref. Lai et al. (2011) and SKC (simple Kalina cycle)

Fluid	***Configuration***	P_{MAX} ***[MPa]***	T_{MAX} ***[K]***	T_{MIN}***[K]***	η_{TH} ***[%]***
n-Pentane	ORC supercritical	4.38	523.15	358.15	19.1
n-Pentane	ORC supercritical	4.72	523.15	358.15	19.0
n-Pentane	ORC subcritical	2.70	523.15	358.15	18.0
n-Pentane	ORC subcritical	3.03	523.15	358.15	18.5
Ammonia-Water 0.7 [mol$_{NH3}$/mol]	SKC	2.43	523.15	358.15	20.0

Henry and Mlcak, (1996) mentioned that axial or radial flow steam turbines could be adapted for SKC applications, mainly because the ammonia molar fraction is only 5% lower than water, thus increasing the flow duct area and decreasing blade stress. Carbon steel does not require special coatings. However, ammonia is a flammable medium and, despite its narrow ignition concentration rate, an appropriate risk-analysis is required. Another main issue is its toxicity, which requires accurate leakage control and minimization.

3. Integrated Gasification SOFC Simple Kalina Cycle (IGSKC)

3.1 Size of the plant

When biomass is used as energy source, restrictions due to the cultivation area required to ensure the specified fuel flow must be considered. The following equation can be adopted to calculate the area of cultivation of a generic biomass needed to produce a certain amount of electric power:

$$A_{cultivation} = k \frac{36\, P_{el}\, H}{\eta_{th} \beta_{cultivation} LHV} \tag{13}$$

where thermal efficiency η_{th} is defined as

$$\eta_{th} = 100 \frac{P_{el} - P_{aux}}{LHV\, \dot{m}_b} \tag{14}$$

The *k*-factor is a dimensionless coefficient (>1) that considers streets, houses and other crops inside the area. P_{el}, H, η_{plant}, and $\beta_{cultivation}$ are the plant electrical power [MW], operating hours per year, plant efficiency and annual productivity of the cultivation area [ton.ha^{-1}year^{-1}], respectively. *LHV* is the lower heating value of the biomass with consideration of the moisture content.

Table 4 presents the values used in the calculation of 8 MW electric power output with woodchips as the fuel input. Thermal efficiency is not calculated as a prior value but is assumed to be 55% for a generic SOFC plant.

Table 4. Parameters and cultivation area calculation

Parameter	***Value***
H	7000 [h/year]
k	4 [-]
η_{th}	55 [%]
$\beta_{cultivation}$	35 [ton/ha]
P_{el}	8 [MW]
LHV	11400 [kJ/kg]
$A_{cultivation}$	**50 [km^2]**

Table 5. Dried woodchips composition (molar mass)

Element	***Weight [%]***
Carbon (Solid)	48.8
Oxygen	43.9
Hydrogen	6.2
Sulfide (Solid)	0.02
Nitrogen	0.17
Ash	0.01

The main properties of woodchips are listed in Tab. 5. Depending on the time of the year, moisture contents up to 60% can be encountered, which decreases the plant power input. In calculations, a moisture content of 33.2% and a low heat value (dried) of 18.28 MJ/kg are assumed, thus leading to a low heat value (humid) of 11.4 MJ/kg. A major parameter is ash content, which may result in high costs of disposal. Problems associated with fouling and corrosion of the fluid-bed gasifier could occur when chlorine and sulphur traces are present because of their capability of forming hydrochloric and sulfuric acid.

3.2 Suggested plant configuration

The results of the combination of the gasification process with SOFC and SKC in the plant configuration are presented in Fig. 6. Woodchips are supplied to the two-stage gasification plant for wood gas production. The first reactor is responsible for the drying and pyrolysis processes, while the second reactor is the fixed bed gasifier. The drying process is crucial to decrease the moisture content of the woodchips. As reported in Hofmann et al. (2007), the gas produced is pure enough to be fed to a SOFC cell without any problems. However, in this study, a simple hot gas cleaner is used to remove the small amount of sulfur that remains after the gasifier. It is assumed that the desulfurizer works at approximately 240°C. The cleaned fuel is preheated in an anode pre-heater (AP) to 650°C before entering the anode side of the SOFC stacks. The operating temperature of the SOFC stacks and the outlet temperatures are assumed to be 780°C. After the stacks, the burned fuel is used to preheat the incoming fuel to the AP. On the other side of the fuel cell, air is compressed and preheated in a cathode pre-heater (CP) to 600°C before entering the cathode side of the SOFC stacks. Because some fuel is left after the anode side of the SOFC stacks, the rest of the fuel, together with the air coming out of the cathode side, is sent to a burner for further combustion. The off-gases from the burner are sent to the HRSG where a SKC recovers the heat inside the EVA and the SUP. The SKC system layout does not differ from the one previously described. It can be noted that the energy of the off-gases from HRSG is further utilized in a HR to preheat the air after the compressor of the SOFC cycle. This technique allows the recycling of heat back to the SOFC cycle, as described by Rokni (2010).

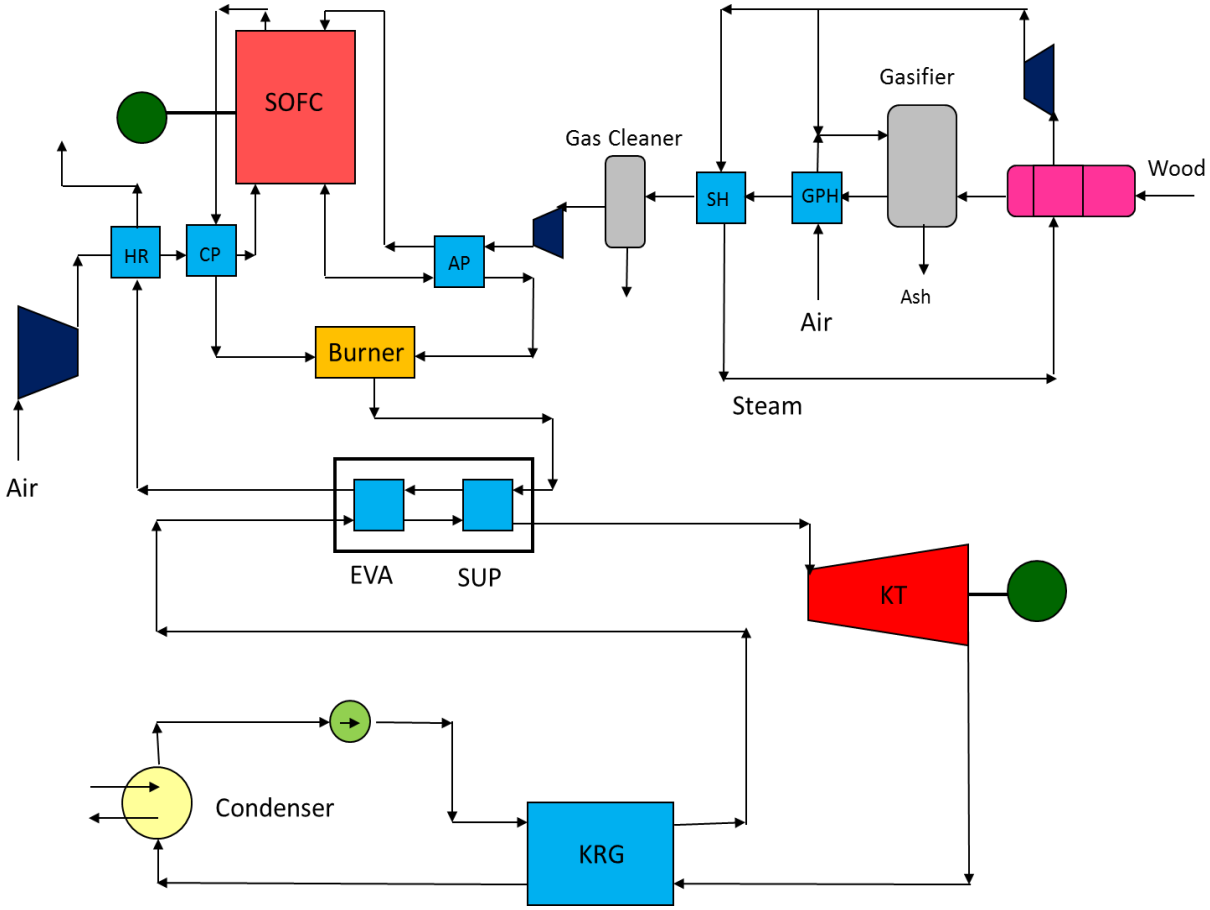

Figure 6. System layout for Integrated Gasification SOFC Kalina Cycle (IGSKC)
AP= Anode preheater, CP=cathode preheater, EVA=evaporator, GPH=gasifier preheater, KRG=Kalina regenerator, KT=Kalina turbine, SH=steam heater, SUP=super heater

The main parameters for the plant are shown in Tab. 6. Pressure drops are the set values for the program; however, pressure drops are a function of channel size and mass flows, and the channel geometry is not known. Calculations show that the final values in terms of power output and efficiency do not differ significantly if these values are slightly changed. The HRSG terminal temperature (off-gases side) is assumed to be 90°C, while the SUP approach point and the EVA pinch point temperature are set to 10°C and 15°C, respectively, to match the HRSG temperature profiles.

Table 6. Plant simulation parameters

Parameter	***Value***
Wood chips temperature	15 [°C]
Wood chips mass flow	1.2 [kg/s]
Dry wood temperature	150 [°C]
Gasifier temperature	800 [°C]
Gasifier pressure drop	0.05 [bar]
Gasifier carbon conversion factor	1
Gasifier non-equilibrium methane	0.01
Steam blower isentropic efficiency	0.8
Steam blower mechanical efficiency	0.98
Steam temperature in the steam loop	150 [°C]
Wood gas blower isentropic efficiency	0.9
Wood gas blower mechanical efficiency	0.98
Gas cleaner pressure drop	0.0049
Compressor air inlet temperature	15 [°C]
Compressor isentropic efficiency	0.85
Compressor mechanical efficiency	0.98
SOFC cathode inlet temperature	60 [°C]
SOFC anode inlet temperature	650 [°C]
SOFC operating temperature	780 [°C]
SOFC utilization factor	0.85
SOFC current density	300 [mA/cm^2]
Heat exchanger fuel side pressure drop ratio	0.005
Heat exchanger air side pressure drops	0.01
Burner pressure drop	0.98
Water side pressure drop in superheater	0.02 [bar]
Water side pressure drop in evaporator	0.03 [bar]
HRSG outlet temperature	90 [°C]
Kalina Turbine isentropic efficiency	0.85
Inlet KT pressure	23.4 [bar]
SUP approach point	15 [°C]
EVA pinch point	10 [°C]
KRG pinch point limit	10 [°C]
DC/AC converter and generator efficiency	0.97
Pump efficiency	0.65

Three simulations are run with different ammonia-water compositions (case A 60%, case B 70% and case C 80%) with the KT inlet pressure set to 23.7 bar. To obtain saturated liquid at 25°C, the condenser pressure is adjusted for each case. The main results and parameters are listed in Tab. 7.

Table 7. Simulation parameters and results for cases A, B, and C

	Case A	***Case B***	***Case C***
Parameters			
x [kmol(NH_3)/kmol]	0.6	0.7	0.8
KT outlet pressure [bar]	4.8	6.4	7.6
Results			
Net power output [MW]	7.30	7.25	7.14
Output power from SOFC cycle [MW]	6.00	6.00	6.00
Output power from SKC cycle [MW]	1.29	1.25	1.13
Thermal efficiency of SKC [%]	21.5	20.8	18.8
Overall thermal efficiency [%]	50.6	50.2	49.4

Figure 7 shows the HRSG heat-temperature profiles of the off-gases and ammonia-water for each case. With fixed 60% percent ammonia in the working fluid, the thermodynamic mean temperature is the highest, resulting in enhanced SKC thermal efficiency. It can be stated that, for the given SUP and EVA approach and pinch point, the optimized ammonia-water percentage is 60%.

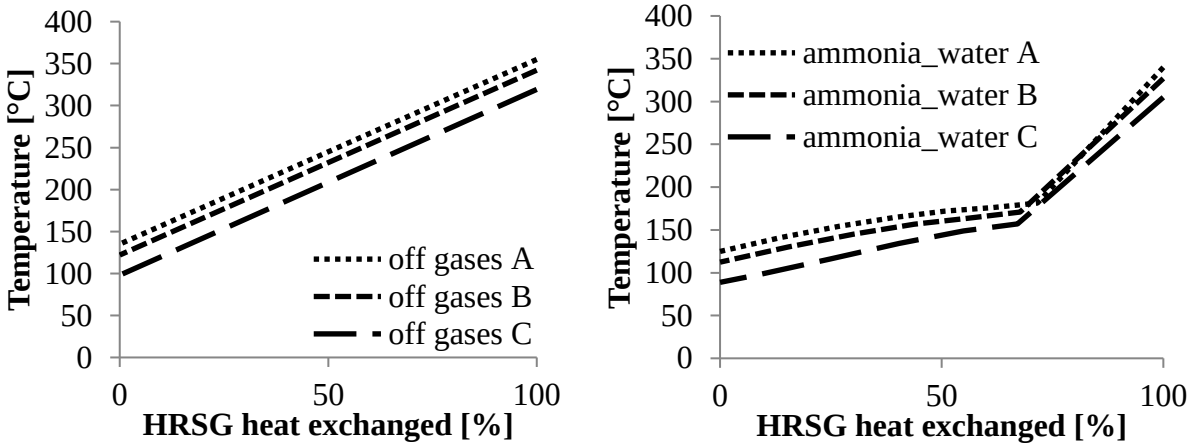

(a) *(b)*

Figure 7. (a) Off-gases temperature vs. heat exchanged in the HRSG (Heat Recovery Steam Generator) for cases studied; (b) Ammonia-water temperature vs. heat exchanged for cases studied

Figure 8 shows the SKC condenser heat-temperature profile with a fixed percentage of 60% ammonia in the working fluid. It can be noted that half of the cooling is due to heating up and partially vaporizing the pumped mixture, and the other half is released to the environment through the condenser.

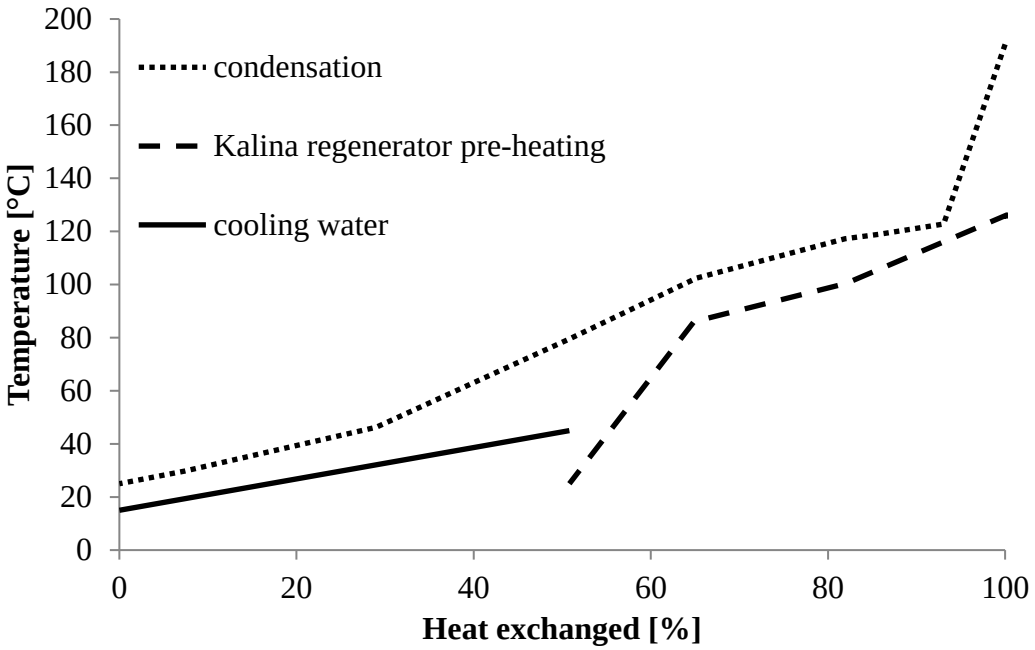

Figure 8. Ammonia-water temperature vs. condenser and Kalina regenerator (KRG) heat exchanged

3.2 Comparison with IGSS solution

In Rokni and Pierobon (2011), a hybrid SOFC and ST plant was integrated with a gasification plant, and the plant was also fired by woodchips. Different system layouts are presented and investigated, and an overall thermal efficiency of 56% was mentioned. The SC heat recovery is compared with the present solution for a fixed ammonia percentage (60%) in the solution. The plant layout and parameters are acquired from Fig. 1 and Tab. 1 (Rokni and Pierobon 2011); a maximum SC pressure of 23.4 bar is selected.

Figure 9 shows the HRSG temperature profile vs. heat exchanged for SC and SKC. It can be noted that, with SC, heat is recovered at a higher temperature, thus increasing the total available work. With regards to the SKC solution, it is confirmed that the HRSG exergy loss is decreased because of the better matching between the off-gases and the ammonia-water temperature profile. However, as denoted in Tab. 8, the bottoming cycle thermal efficiency is lower in the case for SKC than the SC case, which can be explained by lower available heat in the bottoming cycle caused by the hybrid recuperator.

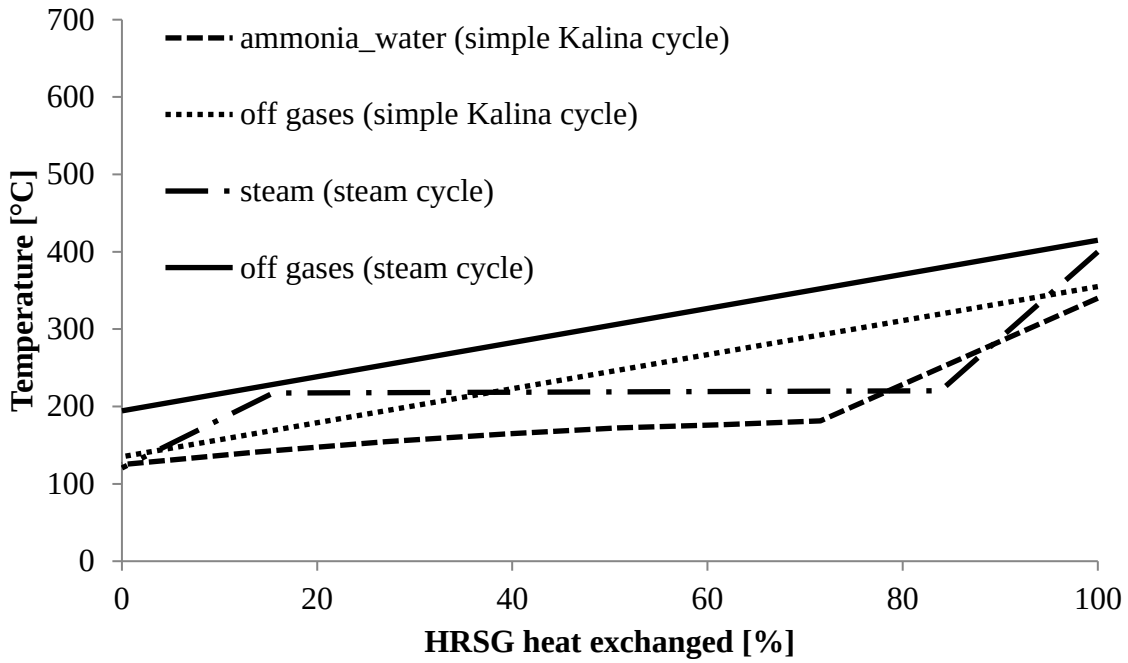

Figure 9. HRSG (heat recovery steam generator) temperature profile as a function of heat exchanged for SKC (simple Kalina cycle) and SC (steam cycle)

Table 8. Simulation parameters and results for steam cycle and simple Kalina cycle

Parameters	***Simple Kalina Cycle*** Tab. 6	***Steam Cycle*** Tab. 1 in ref. Rokni and Pierobon (2011)
Net power output [MW]	7.30	7.66
Output power from SOFC cycle [MW]	6.00	6.01
Output power from SKC cycle [MW]	1.29	1.65
Thermal efficiency of SKC [%]	21.5	26.6
Steam turbine outlet quality	–	93.5
Overall thermal efficiency [%]	50.6	52.5

The potential of the hybrid recuperator to suit the off-gases temperature profile for the specific working fluid makes the SC solution more attractive in terms of overall thermal efficiency. Mainly, the off-gases temperature profile is increased to maintain the SUP and EVA approach and pinch point at the specified values, thus allowing heat to be recovered to the SC at a higher temperature. Additionally, it must be considered that the turbine outlet moisture content is crucial for component lifespan and performance. As listed in Tab. 8, with a maximum pressure of 23.4 bar, a moisture content of 93.5 % vapor is encountered, and the lower limit must be 86%.

3.3 Effects of SOFC operating temperature

The plant with the SKC mixture composition of 60% ammonia is selected for further study, wherein the utilization factor and current density of SOFC stacks are set to 0.9 and 100

mA/cm^2, respectively. The results of the simulations are shown in Tab. 9 where 780°C and 650°C scenarios are considered. With current technology (780°C), a plant efficiency of 58.3% is achieved; for a future scenario (650°C), the plant efficiency is expected to reach 49.7%. Those values are considerably higher than the traditional combined cycle plant with integrated gasification. The ammonia-water pressure is set to 23.4 bar. For the 780 °C case, approximately 87.1% of the total net power output comes from the SOFC plant; in the future scenario, this value is 82.8%.

Table 9. Calculated net power outputs for different scenarios

Parameters/Case	***780 [°C]***	***650 [°C]***
Inlet KT pressure	23.4 [bar]	23.4 [bar]
Net power output	8.32 [MW]	7.22 [MW]
SOFC power output	7.25 [MW]	5.98 [MW]
SKC power output	1.06 [MW]	1.24 [MW]
SOFC cell voltage	0.883 [V]	0.720 [V]
Off gases outlet temperature	90 [°C]	90 [°C]
SKC thermal efficiency	21.6 [%]	21.5 [%]
IGSKC thermal efficiency	58.3 [%]	49.7 [%]

By lowering the operating temperature of SOFC, the IGSKC thermal efficiency decreases by approximately 9%. This effect is mainly due to higher ohmic losses in SOFC cells. However, the lowering operating temperature involves the use of a different material as the electrolyte, meaning that the price is significantly lowered.

4. Conclusions

Hybrid combined IGSKC plants are presented and analyzed for conversion of biomass to electricity. The plants are fired by woodchips; therefore, the fuel is gasified, purified and then sent to the anode side of the SOFC. Additional heat is recovered by the bottom SKC. The size of the plant is selected according to cultivation area requirements.

Three different cases are analyzed based on different ammonia-water percentages in the SKC. It is demonstrated that the optimal ammonia-water fraction is 60%. The results indicate that, for simple combinations, the thermal efficiency of the system can reach approximately 49%-51%, depending on the ammonia percentage in the SKC working fluid. A maximum efficiency of 58.3% is obtained by improving the SOFC utilization factor (0.9) and decreasing the current density (100 A/mm^2). For the future scenario, decreasing the SOFC operation temperature to 650°C would result in an overall performance efficiency of 49.7%. The calculated values are remarkably high in comparison with typical values achieved by biomass to electricity conversion systems.

A comparison with the IGSS system proves that the HR provides a crucial benefit, i.e., heat is recovered by generating steam at a higher mean temperature, thus increasing the SC available work and, consequently, the overall plant efficiency. However, it is confirmed that the use of SKC is suitable for medium and low temperature heat sources when compared to ORC (n-Pentane). The main reason is improved fit between the heat source and the SKC temperature profiles.

5. References

Achenbach, E. (1994). Three-dimensional and time-dependent simulation of a planar solid oxide fuel cell stack. *Journal of Power Sources* 49(1-3); 333–348.

Bang-Møller C. and M. Rokni. (2010). Thermodynamic performance study on biomass gasification, solid oxide fuel cell and micro gas turbine hybrid systems. *Journal of Energy Conversion and Management* 51; 2330–2339.

Bang-Møller C., M. Rokni and B. Elmegaard. (2011) Exergy analysis and optimization of a biomass gasification, solid oxide fuel cell and micro gas turbine hybrid system. *Journal of Energy* 36; 4740–4752.

Calise F., M.D. d' Accadia, L. Vanoli and M.R. von Spakovsky. (2006). Single-level optimization of hybrid SOFC–GT power plant. *Journal of Power Sources* 159; 1169–1185.

Cocco D., C. Palomba and P. Puddu. (2010). Tecnologie delle energie rinnovabili, SGE Editoriali, Padova, ISBN-8889884169.

Di Pippo R. (2004). Second law assessment of binary plants generating power from low-temperature geothermal fluids. *Journal of Geothermic* 33; 565–586.

Dunbar W.R., N. Lior and R.A. Gaggioli. (1991). Combining fuel cells with fuel – fired power plants for improved exergy efficiency. *Journal of Energy* 16(10); 1259–1274.

Elmegaard B. and N. Houbak. (1999). On the Implementation of Energy Simulators with Emphasis on Chemical Equilibrium Gasifier Models. Proceedings of ECOS'99 (ISBN: 4-9980762-0-5); 258–263, Tokyo, Japan.

Elmegaard B. and N. Houbak. (2005). DNA–A general energy system simulation tool. Proceeding of SIMS 2005, Trondheim, Norway.

Ghirardo F., M. Santin, A. Traverso and A. Massardo. (2011). Heat recovery options for onboard fuel cell systems. *International Journal of Hydrogen Energy* 36; 8134–8142.

Henriksen U., J. Ahrenfeldt, T.K. Jensen, B. Gøbel, J.D. Bentzen, C. Hindsgaul, et al. (2006). The design, construction and operation of a 75 kW two-stage gasifier. *Journal of Energy* 31; 1542–1553.

Henry A. and P.E. Mlcak. (1996). An introduction to the Kalina cycle, *PWR* 1996;30, Proceedings of the International Joint Power Generation Conference, October, Huston, Texas, USA.

Hofmann P., A. Schweiger, L. Fryda, K.D. Panopoulos, U. Hohenwarter, D. Bentzen, et al. (2007). High temperature electrolyte supported Ni-GDC/YSZ/LSM SOFC operation on two-stage Viking gasifier product gas. *Journal of Power Sources* 173; 357-366

Jonnson M. and J. Yan. (2000). Exergy and pinch analysis of diesel engine bottoming cycles with ammonia–water mixtures as working fluid. *Journal of Applied Thermodynamics* 3; 57–71.

Keegan K.M., M. Khaleel, L.A. Chick, K. Recknagle, S.P. Simner and J. Diebler. (2002). Analysis of a planar solid oxide fuel cell based automotive auxiliary power unit. *SAE Technical Paper Series* No. 2002-01-0413.

Kim J.W. and A.V. Virkar. (1999). The effect of anode thickness on the performance of anode – supported solid oxide fuel cell. Proc of the Sixth Int Symp On SOFCs, (SOFC – VI); PV99 – 19: 830 – 839, The Electrochemical Society.

Klein S.A. and O.M. Ibrahim. (1993). Thermodynamic properties of ammonia-water mixture. *ASHRAE Transactions*, Symposia CH-93-21-2; 1495–1502.

Lai N.A., M. Wendland and J. Fischer. (2011). Working fluids for high-temperature organic Rankine cycles. *Journal of Energy* 36; 199–211.

Leibowitz H. and M. Mirolli. (1997). First Kalina combined-cycle plant tested successfully. *Journal of Power Engineering* 101(5); 45–48.

Liso V., M.P. Nielsen and S.K. Kær. (2009) Operation strategy for solid oxide fuel cell systems for small-scale stationary applications. *International Journal of Green Energy* 6(6); 583–593.

Marston C.H. (1990). Parametric analysis of the Kalina cycle, *ASME Journal of Engineering for Gas Turbine and Power* 112; 107–116.

Min K., C.W. Sun, W. Qu, X.G. Zhang, S. Yick, M. Robertson, C. Decès-Petit and R. Hui. (2009). Electrochemical properties of low-temperature solid oxide fuel cells under chromium poisoning conditions. *International Journal of Green Energy* 6; 627–637.

Odukoya A., I. Dincer and G.F. Naterer. (2011). Exergy Analysis of a gasification-based combined cycle with solid oxide fuel Cells for cogeneration. *International Journal of Green Energy* 8; 834-856.

Park Y.M. and R.E. Sonntag. (1990). Thermodynamic properties of ammonia water mixture: A generalized equation of state approach. *ASHRAE Transaction* 96; 150–159.

Pruβ A. and W. Wagner. (1995). Eine neue fundamentalgleichung für das fluide zustandsgebiet von wasser für temperaturen von der schmelzlinie bis zu 1273 K bei Drüken bis zu 1000 MPa, Fortschr.-Bcr. *VDI* 6, No. 320, Düsseldorf.

Proell T., R. Rauch, C. Aichering and H. Hofbauer. (2004). Coupling of biomass steam gasification and an SOFC–GT hybrid system for highly efficient electricity generation. ASME Turbo Expo Proceeding GT2004-53900; 103–109.

Pålsson J., A. Selimovic and L. Sjunnesson. (2000). Combined solid oxide fuel cell and gas turbine system for efficient power and heat generation. *Journal of Power Sources* 86; 442–448.

Rokni M. (2010). Thermodynamic analysis of an integrated solid oxide fuel cell cycle with a rankine cycle. *Journal of Energy Conversion and Management* 51(12); 2724–2732.

Rokni M and L. Pierobon. (2011). Integrated gasification SOFC plant with a steam plant. Risø International Energy Conference 2011; 288–297.

Rokni M. (2012). Thermodynamic investigation of an integrated gasification plant with solid oxide fuel cell and steam cycle, *Journal of Green* 2; 71–86.

Rose L., O. Kesler, C. Decès-Petit, T. Troczynski and R. Maric. (2009). Characterization of porous stainless steel 430 for low- and intermediate-temperature solid oxide fuel cell (SOFC) substrates. *International Journal of Green Energy* 6; 638–645.

Smith J.M., H.C. Van Ness and M.M. Abbott. (2005). Introductiosn to chemical engineering thermodynamics, 7th ed., Boston McGraw-Hill.

Subramanyan K. and U.M. Diwekar. (2005). Characterization and quantification of uncertainty in solid oxide fuel cell hybrid power plants. *Journal of Power Sources* 142; 103–116.

Tillner-Roth R. and G. Friend. (1998). A Helmholtz free energy formulation of the thermodynamic properties of the mixture {water + ammonia}. *Journal of Physical and Chemistry Reference Data* 27(1); 63–69.

Tillner-Roth R., F. Harms-Watzenberg and H.D. Baehr. (1993). Eiene neue fundament-algleichung für ammoniak. *DKV Tagungsbericht* 20 (2//PT1); 67.

Zhang X., M. He and Y. Zhang. (2012). A review of research on the Kalina cycle. *Journal of Renewable and Sustainable Energy Reviews* 16; 5309–5318.

Zhu H. and R.J. Kee. (2003). A general mathematical model for analyzing the performance of fuel-cell membrane-electrode assemblies. *Journal of Power Sources* 117(1–2); 61–74.